Characterization of Reverberation Chamber - A Comprehensive Review

JAWAD YOUSAF[1], **WANSOO NAH**[2], (Member, IEEE),
MOUSA I. HUSSEIN[3], (Senior Member, IEEE), **JUN GYU YANG**[4],
AMIR ALTAF[2], (Member, IEEE), **AND MANZOOR ELAHI**[5]

[1]Department of Electrical and Computer Engineering, Abu Dhabi University, Al Ain 1790, United Arab Emirates
[2]Department of Electrical and Computer Engineering, Sungkyunkwan University, Seoul 561-758, South Korea
[3]Department of Electrical Engineering, United Arab Emirates University, Al Ain 15551, United Arab Emirates
[4]National Radio Research Agency (RRA), Naju 58323, South Korea
[5]Department of Electrical and Computer Engineering, COMSATS University, Islamabad 45550, Pakistan

Corresponding authors: Jawad Yousaf (jawad.yousaf@adu.ac.ae) and Wansoo Nah (wsnah@skku.edu)

ABSTRACT This study presents a comprehensive review of the characterization techniques of a reverberation chamber (RC). After describing the limitations of the theoretical models for the determination of the lowest usable frequency (LUF) of a chamber, the normative procedure of IEC 61000-4-21 standard is summarized for the estimation of LUF of an RC. Then a brief overview of the recent approaches for the full-wave EM modeling and characterization of EM fields in an RC using statistical tests is presented. The study also discusses the limitations of conventional field uniformity based RC calibration procedure with a review of the recently proposed fast indirect validation procedure of RC using S-parameters measurements. Lastly, this work reviews the estimation of the RC quality factor (Q-factor) using analytical, time-and frequency-domain techniques and their limitations.

INDEX TERMS Reverberation chamber (RC), IEC 61000-4-21, S-Parameters, RC calibration, 3D Model, stirrer/tuner, lowest usable frequency (LUF), field uniformity, statistical test, AD-GOF test, quality factor (Q), time-domain Q, frequency-domain Q, composite Q, RC losses.

I. INTRODUCTION

Reverberation chamber (RC) was first introduced by H. A. Mendes in 1968 [1]. Since more than 40 years, RC is being used extensively for the wide range of radio frequency application, such as antennas and sensors characterization [2]–[6], electromagnetic- interference (EMI) and -susceptibility (EMS) measurements [7], shielding and absorption cross-section (ACS) characterization of materials [7], realization of multipath channel environment [8]–[11], and the over-the-air (OAT) tests for the future 5G/6G devices [5].

The basic components of a reverberation chamber are a highly-conductive and electrically large shielded metallic cavity structure, a tuner/stirrer, and transmit (Tx) and receiver (Rx) antennas. The electromagnetic (EM)

The associate editor coordinating the review of this manuscript and approving it for publication was Amedeo Andreotti.

environment inside the reverberation chamber is varied using different kinds of stirring techniques such as tuner movement (mode-tuned or mode-stirred), frequency stirring, the vibration of a conductive cloth, variations of orientation, polarization or position of used antennas or equipment under test (EUT) [11]–[16]. Either one or combination of the aforementioned stirring techniques are employed to vary the modal structure inside the RC for the generation of the statistically uniform, isotropic, and homogeneous spatial EM fields inside the RC [12], [15], [17].

The RC offers comprehensive advantages of generation of high field strength with a moderate input power, shorter testing time, large testing volume, and no EUT rotation requirements as compared to open area test sites (OATS) and semi/full anechoic chambers [5], [18]–[21]. The assurance of spatial field uniformity depicting the overmoded or well-stirred condition of RC is essential before the conduction of any kind of testing in an RC. Different kind of
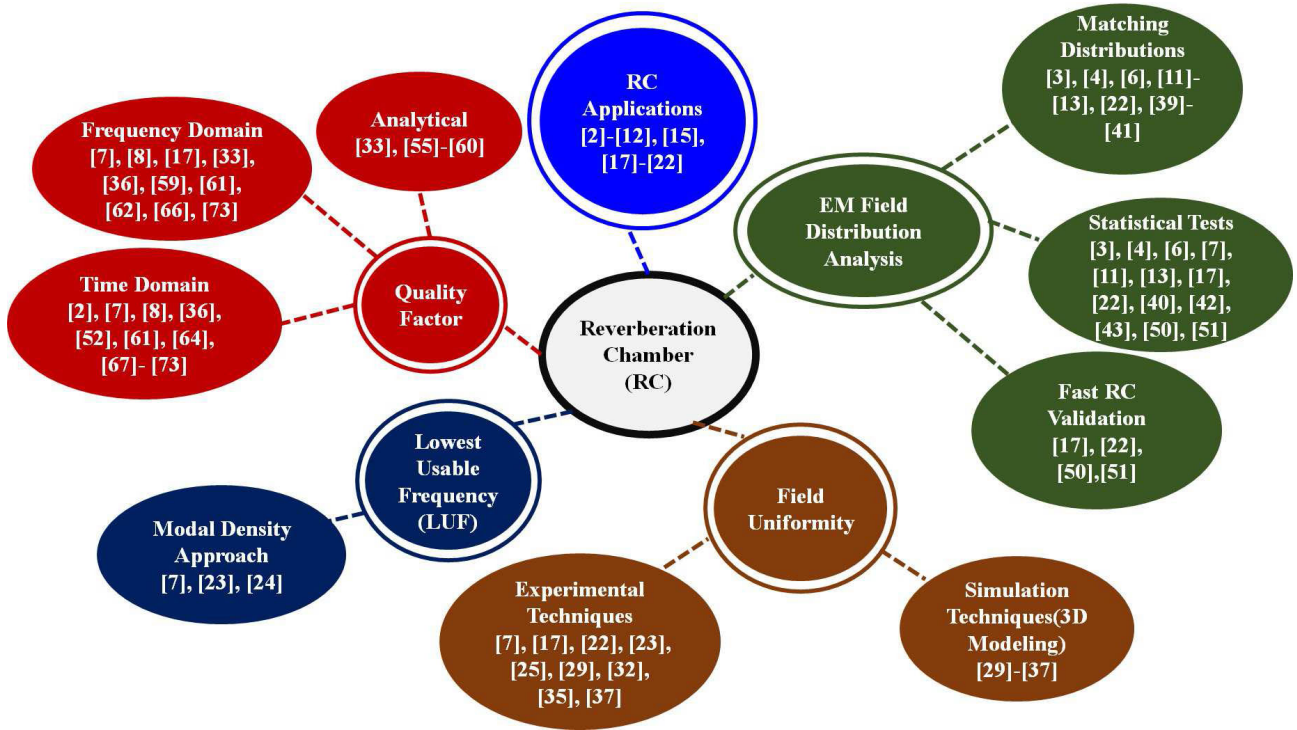
FIGURE 1. Graphical summary of reviewed topics for RC characterization.

conventional long time-taking normative procedure [3], [7] and fast *S*-parameters based methods [17], [22] are used for the characterization of the well-stirred condition of the RC. The purpose of performing such tests is to determine the lowest usable frequency (LUF) or well-stirred frequency of the chamber after which desired testings can be conducted in an RC.

This work presents a comprehensive review of the various characterization techniques of the RC. The study starts with a brief review of theoretical modeling of the RC spectrum and determination of the LUF of an RC using analytical models of modal density and their limitations (Section II). After that details of the normative procedure of International Electrotechnical Commission (IEC) 61000-4-21 based on EM field uniformity is outlined in Section III for the estimation of LUF based on measured EM fields in an RC. Next, the various recent techniques used for simulation based analysis of RC field distribution using full-wave EM modeling of an RC are discussed. Section IV summarizes the various statistical procedure for the characterization of the EM field distribution of an RC. The discussion about the limitations of the conventional field uniformity based RC calibration procedure and newly proposed fast indirect characterization of the well-stirred condition of RC using *S*-parameter measurements (field distribution analysis) is included in Section IV. After that, the study discussed the analytical and time- and frequency-domain techniques and their limitations for the estimation of the quality factor (*Q*) and time constant of

an RC in Section V. Figure 1 summarizes the reviewed topics for the characterization of an RC.

II. LOWEST USABLE FREQUENCY OF RC
Lowest usable frequency (LUF) is the frequency at which the chamber meets the operational measurement requirements. The knowledge of the LUF of chamber is essential for the conduction of any kind of testing or measurements in the RC. This section discuss the theoretical techniques for the determination of the lowest usable frequency (LUF) of an RC.

A. THEORETICAL MODAL SPECTRUM ANALYSIS OF RC
The theoretical modal spectrum of a large-sized Korean National Radio Agency (RRA) (9.3 m (*L*) × 6.1 m (*W*) × 4.9 m (*H*)) RC chamber is shown in Fig. 2. We can note that the number of modes in the RC cavity increases with the enhancement of frequency. It is important to note that there can be several modes having the same cut off frequency which are referred to as 'degenerate modes' which can be noticed in Fig. 2(a). The fundamental modal frequency of a rectangular cavity can be computed using (1) [7]. In (1), *c* represents the speed of light, *m*, *n*, and *p* are integers, and *L*, *W*, and *H* refer to the length, width, and height of metallic cavity. For the aforementioned RC dimension, the fundamental modal frequency (f_{110}) of this RC is 29.4 MHz as also depicted in Fig. 2(b) as the first cavity resonance mode frequency.

$$f_{mnp} = \frac{c}{2}\sqrt{\left(\frac{m}{L}\right)^2 + \left(\frac{n}{W}\right)^2 + \left(\frac{p}{H}\right)^2} \quad (1)$$
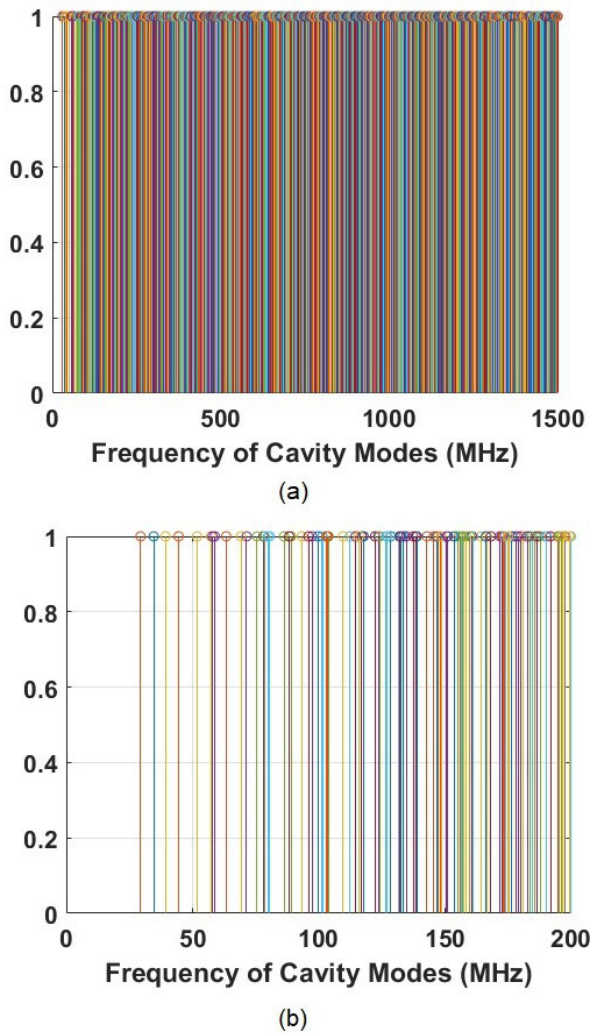
FIGURE 2. Theoretical modal spectrum of RRA RC (a) 0-1500 MHz; (b) 0-200 MHz.

FIGURE 3. Variations in the number of modes and modal density in RRC RC [23].

B. DETERMINATION OF LUF USING MODAL DENSITY

In practice, typically LUF occurs at a frequency slightly above three times of the first chamber modal resonance. LUF can also be expressed as; (i) frequency at which at least 60-100 modes exist inside the cavity; (ii) frequency at which at least 1.5 mode/MHz (modal density) are present inside the cavity [7], [23]. These typical limits are formed to ensure that there are a sufficient number of modes in RC to meet the essential operational requirements of statistically uniform and homogenous fields.

Undermoded cavity is the case when the RC is working below the LUF. The overmoded or stirred condition occurs when the RC operates after the LUF. The presence of the large number of modes makes the RC operation as overmoded. Normally the field in the undermoded cavity is considered as the unstirred field due to the presence of a fewer number of modes. However, the direct coupling between antennas [13] can introduce the unstirred field components in the stirred/overmoded region.
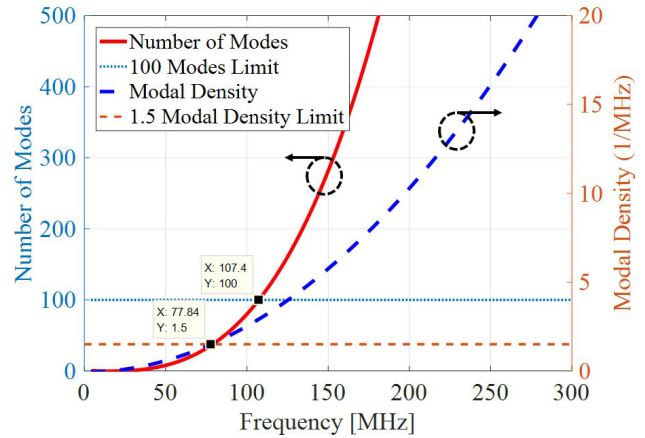
The generalized Weyl formula for the number of modes ($N(f)$) calculations (2) or modal density (m) (3) [24] are used for the rough estimation of LUF of an RC based on its geometrical dimensions. For example, the computed LUF using the number of modes (2) and modal density formula of (3) are around 108 MHz and 78 MHz, respectively (see Fig. 3) for the RRA RC. These results illustrate that the LUF using modes information here refereed to as $f_{LUF_{MD}}$ of RRA RC is around 78-108 MHz.

$$N(f) \approx \frac{8\pi}{3} \times LWH \times \left(\frac{f}{c}\right)^3 - (L + W + H) \times \frac{f}{c} + \frac{1}{2}$$
(2)

$$m\left(\frac{\partial N}{\partial f}\right) \approx 8\pi \times LWH \times \frac{f^2}{c^3} - (L + W + H) \times \frac{1}{c}$$
(3)

The impact of the RC geometrical structure variations, inherent uncertainties and losses of RC is not incorporated in the modal density formulas of [24] and thus the LUF determined using this way may ($f_{LUF_{MD}}$) not be accurate.

III. FIELD UNIFORMITY

In this section measurements and simulation techniques for the EM field uniformity analysis of an RC are discussed. The EM filed uniformity analysis in terms of its standard deviation could provide more robust estimation of the LUF of an RC.

The estimated LUF using modal densities formulas did not incorporate the inherent uncertainties and RC losses factors in it. A more robust approach to determine the LUF by including the aforementioned factors is the assessment of EM-field uniformity of an RC [7]. The procedure in [7] is also referred to as the conventional approach of RC calibration. The calibration of the RC must be performed using [7] method at least one time in its lifetime. In this work, the LUF determined using the IEC field uniformity assessment procedure is referred to as $f_{LUF_{IEC}}$ for brevity in onward discussions.

A typical setup for the electric field measurements for the field uniformity calculations as per IEC 61000-4-21 requirements [7] is shown in Fig. 4 for an unloaded/empty
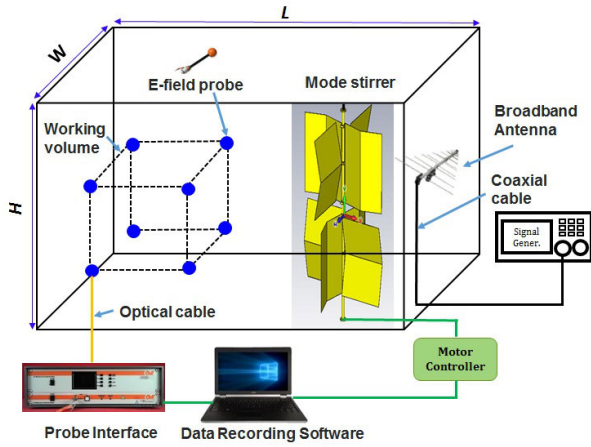
FIGURE 4. A typical simplified setup for the field uniformity measurements as per IEC 61000-4-21 requirements for an empty chamber.

FIGURE 5. A typical experimental setup for field uniformity measurements as per IEC 61000-4-21 requirements for an empty chamber.

TABLE 1. Field uniformity data measurement requirements of IEC 61000-4-21 standard [7].

Frequency range	Minimum number of samples of stirrer rotation	Number of frequencies (log spaced) required for validations/decade
f_s - $3f_s$	12	20
$3f_s$-$6f_s$	12	15
$6f_s$-$10f_s$	12	10
>$10f_s$	12	20
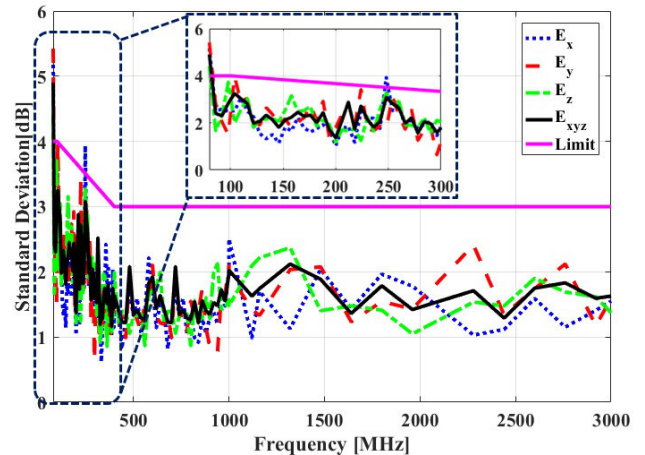
FIGURE 6. Field uniformity results for a typical large size RC.

chamber. The real measurement setup picture of the RRA RC is depicted in Fig. 5. The RC is excited with a broadband antenna placed towards the corner of the RC. A working volume is defined by keeping at least $\lambda/4$ (where λ is the wavelength at the lowest frequency for which calibration is being performed) distance away from the chamber walls and any other metallic object such as stirrer or transmitting antenna. The three dimensional E-field Cartesian rectangular components (E_x, E_y and E_z) at 8 or 9 points within the specified working volume of the chamber are measured using tri-axial probes for different positions of the rotating stirrer. The measurements are conducted as per the defined minimum number of stirrer step size and the number of frequencies in Table 1. After that standard deviation of each rectangular and combined components of electric field is calculated using (4) and (5). In (4), $\overset{\leftrightarrow}{E_i}$ and $\left\langle \overset{\leftrightarrow}{E} \right\rangle$ represent the normalized and averaged value of each E-field component respectively. The determined values are compared with the frequency-dependent threshold criteria of the standard to determine the LUF of the chamber [7].

$$\sigma = \sqrt{\frac{\left(\sum \left(\overset{\leftrightarrow}{E_i} - \left\langle \overset{\leftrightarrow}{E} \right\rangle \right)^2 \right)}{n-1}}$$
$$i = x, y, z \qquad (4)$$

$$\sigma_{dB} = 20 log_{10} \left(\frac{\sigma + \left\langle \overset{\leftrightarrow}{E}_{x,y,z} \right\rangle}{\left\langle \overset{\leftrightarrow}{E}_{x,y,z} \right\rangle} \right) \qquad (5)$$

Figure 6 illustrates the measured field uniformity standard deviation results for a typical large size RRA RC in the frequency range of 80 MHz to 3000 MHz. The E-fields are measured at the eight corners of the working volume of size 4 m × 3 m × 2 m, for the 50 rotations ($N = 50$) of the one large stirrer in RC, as depicted in Figs. 4 and 5. The LUF is the frequency after which the standard deviation of magnitude
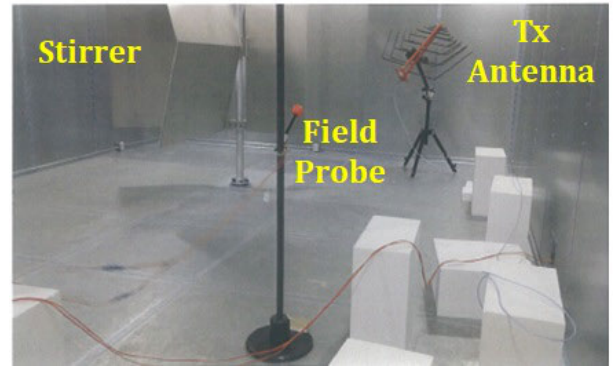
of all rectangular components of E-field *i.e.* E_x, E_y, E_z, and combine E_{xyz} is lower than defined threshold limit in [7].

Figure 6 shows that the $f_{LUF_{IEC}}$ of this chamber based on field uniformity measurements is around 250 MHz. This computed value of $f_{LUF_{IEC}}$ is much higher than the previously predicted LUF using modal density formulas *i.e.* $f_{LUF_{MD}}$ in Section II-B. The inclusion of RC inherent losses and uncertainties in the measured E-field data shifts the LUF to higher frequency compared to theoretical formulas of (2) and (3).

The method in [7] has a great advantage of the simple and easy to follow procedure for the assessment of field uniformity of RC. However, this traditional method of calibration

using field uniformity assessment has disadvantages in terms of long calibration time as each Cartesian rectangular component of the E-field has to be measured for each frequency as outlined in [7]. The collection of E-field data for multiple probe positions for each frequency sample along with slow response time of conventional E-field probes requires long time (up to a week as mentioned in [17], [22], [25]) for the calibration of RC even with fewer number of frequency samples. The utilization of multi-probe system for the simultaneous measurements of E-fields as proposed in [25] (see Fig. 7) can reduce the measurement time as compared to [7] at the cost of the optically fed high sensitive expensive 3D multi-probe system. Nevertheless, the procedure in [7] has to be repeated for any modification in chamber either in the form of change in stirrer type, number of stirrers, posting of stirrers, working volume size or adding of additional load to check for optimal chamber loading which makes the job quite tedious.

FIGURE 7. Multi-probe setup in a classical RC [25].

The experimental characterization of the reverberation chamber analyzes the field uniformity of the RC. To get more insight into the changing boundary conditions with the variations in the stirring technique and its affect on the EM field of an RC, full-wave numerical model of RC ware developed. A typical 3D model of an RC is shown in Fig. 8.

The source of an RC is usually defined in the form of a broadband antenna. A working volume is defined as the region which is $\lambda/4$ away from any metallic surface (RC walls, stirrer, antenna) in an RC. The 8/3 electric field probes are placed at the corners of the working volume for the recording of E-field data as depicted in Fig. 8. A stirrer is a very important part of the RC and it must be modeled accurately for robust and reliable characterization of the
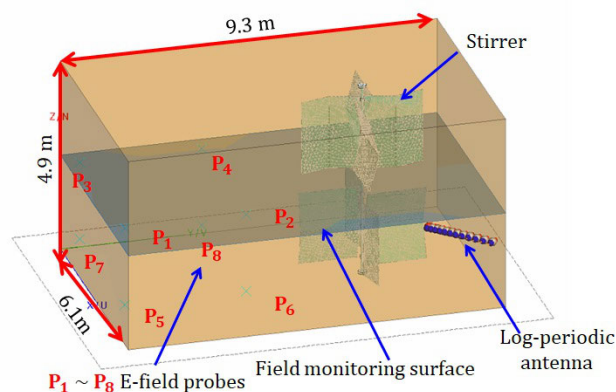
FIGURE 8. Full wave numerical model of an RC [23].

RC performance. 3D modeling also allows us to instigate the changing EM field in an RC by defining various field monitoring surfaces at different locations in RC. The additional provided advantages of full-wave numerical modeling of the chamber are an easy investigation of chamber performance in terms of change in its dimensions, shape, working volume size, wall materials, stirrer shape, size, and installation position, number of stirrers, and door shape and position *etc.* [26]–[28].

A wide range of full-wave EM models of RCs are reported in literature based on both time- and frequency-domain modeling techniques. Asander *et al.* [29] analyzed the impact of two different stirrer designs on the field uniformity of a mode stirred RC using Boundary Element Method (BEM) based on Electric Field Integral Equation (EFIE). An initial detailed study about the complete 3D modeling of a medium-sized RC using method-of-moments (MOM) technique with a detailed analysis of the effect of a door, stirrer, and wall materials on the field in an RC is done by [26]. In [27], the authors analyzed the impact of the multiple different kinds of stirrers in the field uniformity of an RC at low frequency. The impact of four various configurations of two installed tuners (2-plate and 6-plate tuners) on the changing EM-field in an RC for a fixed frequency using the MOM approach is reported in [28]. Moglie *et al.* [30], [31] modeled the RC using discrete plan wave representation using their own developed FDTD code for the study of Anderson darling (AD) rejection frequencies and determination of new location of working volume in the stirrer rotating volume.

Another small-size RC modeling analysis for a fixed frequency using dipole antenna as excitation source is reported in [32]. Aizan *et al.* [34] investigated the impact of three different stirrers (flat panel, irregular Z-folded, and asymmetrical irregular folded) designs on the field uniformity of a medium-sized RC with a monopole antenna as an excitation source. Aditia *et al.* [35] analyzed the medium-sized KRISS reverberation chamber 1 (KRC 1) with two installed stirrers in FEKO. Recently, [37] reported the analysis of the five different kinds of stirrer on the field distribution of a large-sized RC.

TABLE 2. Summary of reviewed 3D models of RC.

Reference	Year	Simulation Technique	Excitation Antenna	Summary
[29]	2002	MOM	Dipole	o Modeling of RC cavity with loss tangent of $1/Q$ to incorporate losses o Analysis of the stirrer design on field uniformity and quality factor
[26]	2005	MOM	Hertizain dipole, $\lambda/2$ dipole, biconical, logper, and horn	o Detailed 3D modeling of medium-sized RCs o Analysis of the effect of the stirrer, door, and wall material on EM field
[27]	2008	MOM	Yagi-uda	o 3D model of a small size RC o Analysis of three different kinds of stirrers for a fixed frequency in RC on working volume variation
[28]	2009	MOM hybridization with PO, GO, and UTD	–	o 3D model of a small size RC o Analysis of four different kinds of stirrers on field distribution in RC at fixed frequency
[30], [31]	2012	FDTD code	-	o RC 3D modeling based on discrete plan wave representation o Analysis of the various RC factors on the AD rejected frequencies o Analysis of the new location of working volume in RC
[32]	2013	MOM	Dipole	o 3D modeling of small size RC with a simple two-plate stirrer o Fixed frequency field uniformity analysis
[33]	2013	FDTD	Dipole	o 3D model of a RC with different air conductivities to model losses o Analysis of quality factor of RC
[34]	2015	FIT	Monopole	o 3D model of a small size RC o Analysis of three different kinds of stirrers
[35]	2016	MOM	Log-periodic	o 3D modeling of medium-sized RC with two installed stirrers o Analysis of KRISS RC 1
[36]	2016	Cavity-Greens function with moment method	dipole	o 3D modeling of large-sized SMART-80 RC without stirrer o Analysis time-and frequency domain quality factor of RC
[37]	2019	MOM with MLFMM	Log-periodic	o 3D model of a large size RC o Analysis of five different kinds of stirrers on field distribution in RC

Method of moments (MOM), physical optics (PO), geometric optics (GO), multilevel fast multipole method (MLFMM), anderson-Darling (AD), uniform theory of diffraction (UTD), finite-difference time-domain (FDTD), finite-integration technique (FIT), and quality factor (Q)

The conductivity of the wall-materials highly impacts the contribution of the wall-losses in the simulation environment [26], [28], [29], [33]. The achievement of the desired quality factor of an RC is numerical environment demands the modeling of the RC with real conductors which make the numerical model computational inefficient [26], [34], [37]. It has been shown that overall losses of the RC can be accounted in the full-wave simulation by changing the free-space air conductivity to 10^{-5} S/m for aluminum [38] and 2×10^{-5} S/m for galvanized steel [33] while keeping the wall material as perfect electric conductor (PEC). The authors in [29], [36] modeled the loss tangent of the cavity space of the RC as the inverse of the fixed quality factor (Q) to account the wall losses. The adding of the lossy media could reduce the computational resources with minimum impacts on the results and thus provides more realistic modeling of the RC. Table 2 summarizes the reviewed, recently reported, legacy 3D models of an RC.

The analysis of reviewed designs in Table 2 shows that frequency domain MOM approach is the preferred choice for the full-wave EM analysis of an RC [26]–[28], [32], [35], [37]. The hybridization of the MOM with physical optics (PO), geometrical optics (GO), uniform theory of diffraction (UTD), and multilevel fast multipole method (MLFMM) techniques in FEKO offers a comprehensive reduction in the

simulation time of a large size RC cavity [26]–[28], [32], [35], [37]. Despite the RC structure, simulation time highly depends on the used metallic material for the modeling of RC walls, tuner, and antenna structures [26], [34], [35], [37]. The better agreement between the simulated and experimental results of the 3D model of an RC demands the accurate modeling of RC by incorporating even smallest geometrical details (RC geometry, wall materials and thickness, stirrer type, size and its installed positions in RC, door size and its position, and the excitation antenna type *etc.*) in the full-wave EM model of an RC [26], [34], [35], [37].

IV. EM FIELD DISTRIBUTION IN RC

The amplitude of the complex E-field rectangular components in an ideal working (well-stirred/overmoded) RC follows the Rayleigh distribution (or χ distribution with two degrees of freedom) and the samples are uncorrelated with each other [12], [13], [39], [40].

The presence of the unstirred components either due to the undermode (below LUF) operation or due to the direct coupling between the antennas make the RC field distribution as Rician or Rice distribution [3], [13]. The Rician distribution has a non-zero mean of Gaussian field components. Rayleigh distribution is the special case of the Rice distribution when the unstirred component is null. The ratio of the variance (σ)
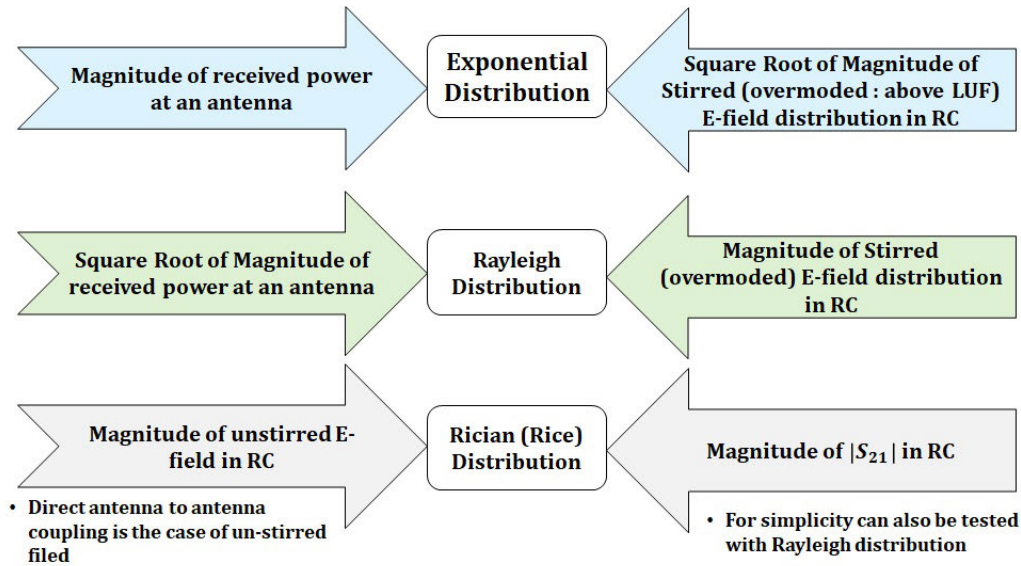
FIGURE 9. Preference of distribution choices for the characterization of RC environment.

and the square of the mean (μ^2) for the Rayleigh distribution is 0.273 [3], [13] while it is approximately 0.52 for σ/μ [3], [40]. It means if the ratio of the sample σ/μ is around 0.52 then it follows the Rayleigh distribution.

Lemoine et al. [40] proposed that Weibull distribution has better fitting to the magnitude of the RC field and received power at an antenna in an overmoded chamber case as compared to conventional Rayleigh distribution. Figure 9 shows preference choice for the selection of the specific distribution for statistical testing. According to Margolin's Lemma [40], testing the Rayleigh distribution on a sample is equivalent to testing the Exponential distribution on the square of the sample.

The summary of distribution choice for the characterization of RC environment is as follows:

- Rayleigh distribution is most commonly used for the testing of stirred (overmoded) EM field magnitude distribution in RC [3], [13], [22], [41].
- The distribution of magnitude of $|S_{21}|$ is more closer to the Rice distribution. However, for brevity, it can also be compared with Rayleigh distribution assuming ideal RC operation (no unstirred component) [22], [41].
- Weibull distribution as proposed by [40] also being considered as a good candidate for the testing of stirred E-field magnitude in RC instead of Rayleigh distribution as it combines the effect of both Rayleigh and Rician distributions.

A. STATISTICAL TESTS FOR RC FIELD ANALYSIS

Different kind of statistical tests are used for the assessment of the distribution of the measured or calculated field, S-parameter data or the received power at an antenna terminal of an RC [6], [11]. The tests are conducted to check the

null hypothesis (H_0) which specifies that the testing sample follows a specified distribution as summarized in Fig. 9. For example magnitude of E-field distribution in RC follows Rayleigh distribution or $|S_{21}|$ follows the Rician/Rayleigh distribution [3], [6], [11].

The statistical tests procedure for the characterization of the RC data can be divided into two branches: hypothesis testing and critical value evaluation. In hypothesis testing the results is only in the form of acceptance or rejection (rejection ratio) of null hypothesis (e.g. $k = 0$ if $|E|$ follows Rayleigh distribution or vice versa). Based on the null hypothesis test results (k value), the moving rejection ratio is computed. While in critical value evaluation, the output test results can be assessed for a certain threshold value which provide better insight for the difference RC studies.

Chi-square (χ^2) test is previously used for RC field analysis [13] but not preferred due to the continuous distribution of the field inside RC [3], [4], [40]. Preferred test for checking of goodness-of-fit of the RC sample data with the required distribution are Anderson-Darling Test (AD Test) and Kolmogorov-Smirnov test (KS test) [4], [40], [42]. The fitting functions are defined for each test type to evaluate the matching of the distribution of the theoretical and measured data in terms of the statistic value. The analysis using critical value (tv_{test}) is preferred because the direct rejecting using the null hypothesis may result in a higher rejection ratio. The critical value is also preferred for the evaluation of the auto-correlation of the E-field or magnitude of transfer coefficient $|S_{21}|$. The first-order auto-correlation (ρ) is used to analyze the requirements of the independent samples of RC is dependent on the number of stirring method variations (N) [7].

Equation (6) represents the KS test statistic value (d) which is the absolute maximum difference of the theoretical ($F(x)$)

and empirical ($S_N(x)$) cumulative distribution function (CDF) of investigating data. Subsequently, the modified test statistics $(d - 0.2/N)(\sqrt{N} + 0.26 + 0.5/\sqrt{N})$ is computed based on the number of stirring condition (N) for comparison with Exponential/Rayleigh distribution. This modified statistic is then compared with the critical value (tv_{test}) limit to accept or reject the null hypothesis [40].

$$d = max \, |F(x) - S_N(x)| \qquad (6)$$

The AD-GOF test statistics expression A^2 is shown in (7) [40]. In (7), theoretical CDF is represented by $F(x_i)$. To calculate the A^2 statistic, the ascending order arrangement of measurement values (x_i) of rank i is formed. Then a modified test statistic value of $A^2(1+0.6/N)$ is computed based on the number of stirring conditions (N). Tables 3 and 4 show the critical values for E-field/S-parameters testing for different specified distributions of Fig. 9 and auto-correlation (ρ) testing for the successive samples of E-field/S-parameters data. The AD-GOF tests provide better results than χ^2- and KS-test due to its intrinsic properties of higher rank and sensitivity to the furthest distribution values [40].

$$A^2 = -\frac{\sum_{i=1}^{N}(2i-1)\left[lnF(x_i) + ln(1 - F(x_{N+1-i}))\right]}{N} - N \qquad (7)$$

TABLE 3. Critical value for KS/AD-GOF testing (tv_{test}) of the magnitude of E-field/S_{21} of an RC environment with the fitting function of each test type [40], [42].

For KS testing of Exponential/Rayleigh distribution [42]				
α	0.15	0.1	0.05	0.025	0.01
tv_{test}	0.64	0.45	0.37	0.32	0.28
For AD-GOF testing of Exponential/Rayleigh distribution [42]				
α	0.15	0.1	0.05	0.025	0.01
tv_{test}	0.922	1.078	1.341	1.606	1.957

For KS/AD-GOF testing of Weibull distribution [40]		
	KS	AD GOF
α	tv_{test}	tv_{test}
0.1	$0.8625 - 0.1991/\sqrt{N}$	0.637
0.05	$0.8982 - 0.2216/\sqrt{N}$	0.757
0.01	$1.0455 - 0.2826/\sqrt{N}$	1.038

TABLE 4. Critical values (tv_r) for the first-order auto-correlation based on N for a confidence level of 95 % [43].

N	10	20	30	40	50	75	100
tv_r	0.64	0.45	0.37	0.32	0.28	0.23	0.2

Figure 10 depicts the comparison of distribution matching of a sample result of the magnitude of E-field and S_{21} data recorded in RRA RC at 92 MHz for 50 steps of stirrer rotations *i.e.* N = 50. The shown results in Fig. 10 are for the AD-GOF testing with the matching of theoretical CDF with measurement values. The critical test value *i.e.* tv_{test} is 1.341 in this case for matching of distribution of these parameters to the Rayleigh distribution with a significance

level (α) of 0.05 (see Table 3). We can observe from Fig. 10(a) that for the for $|E - field|$, the AD-GOF statistics value is 1.8462 which is greater than tv_{test} of 1.341 and thus results in rejection of the null hypothesis here ($k = 1$). Similar results can be observed for $|S_{21}|$ in Fig. 10(b).

The determination of the high-level field which can be produced in an RC is important, particularly for the immunity testings. This is referred to as electric field upper bound and both deterministic and statistical approached are reported for its estimation [44]–[46]. The limitation of the constrained energy in RC makes the statistical approach bounded. The statistical models for the prediction of the maximum E-field using the chamber unconditional probability density function (PDFs) did not have a natural upper bound for a well-stirred field in RC [45]–[49]. The dependency on the attendant PDFs brings a difference between the total maximum electric field value and its single component [45], [48].

In contrast to the statistical approach, Gifuni [44] suggested that the deterministic approach is more appropriate and the upper bound of E-field can be computed from its root mean square (MSV) value only. The MSV can be computed easily by recording the average received powers at the antenna terminal inside an RC or by using an isotropic probe system.

The quick analysis of RC EM field distribution can be performed by comparing the magnitude of transfer characteristics *i.e.* $|S_{21}|$ with Rayleigh distribution. Recently, keeping in view the constrain of long measurements time of [7] calibration procedure, researchers have proposed some alternative indirect methods for the fast calibration of the RC based on S-parameter measurements [17], [22] and coupling transfer gain function ($|T_I(j\omega)|$) [50], [51] of RC environment. Single port [17] or two-port S-parameter measurements [22], [50], [51] are conducted in an RC for this purpose. The typical setup for such measurements using two antennas is illustrated in Fig. 11. Two broadband antennas are placed inside the RC with minimum $\lambda/2$ distance between the two antennas and any other metallic object in RC, such as stirrer and RC walls. Two-port S-parameters are recorded using a vector network analyzer (VNA) by rotating the stirrers in discrete steps for one complete revolution. For one port S-parameter recording [17], second antennas could be removed from the setup of Fig. 11. The quick measurements using VNA for a large number of frequency samples and the desired number of stirrer rotations (N) reduces the measurement time drastically as compared to the experimental time of [7]. The measurements must be performed for the higher number of frequency samples to compensate for the effect that the measurements are not being conducted at several positions within the RC [17].

The principle of reported [17], [22], [50], [51] methods is based on the assessment of the well-stirred condition of RC. As per the definition of the well-stirred operation (wso) of RC defined in [17], [22], [50], [51], the determination of the frequency after which chamber operation ensures spatial field uniformity, isotropy and polarization purity (here referred to
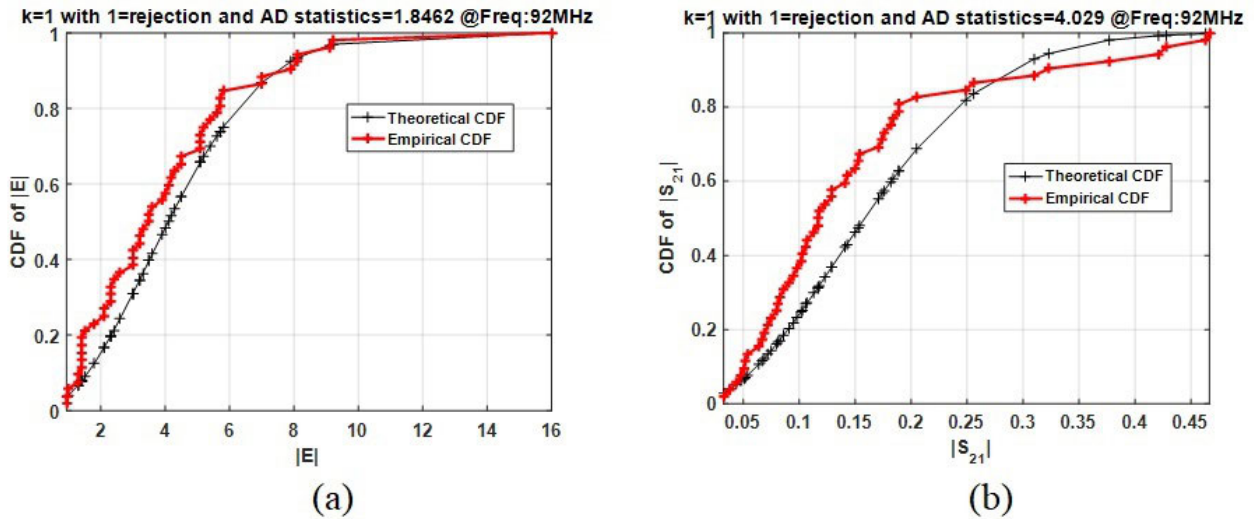
FIGURE 10. Comparison of distribution matching of RC data with Rayleigh distribution (a) $|E - field|$; and (b) $|S_{21}|$.
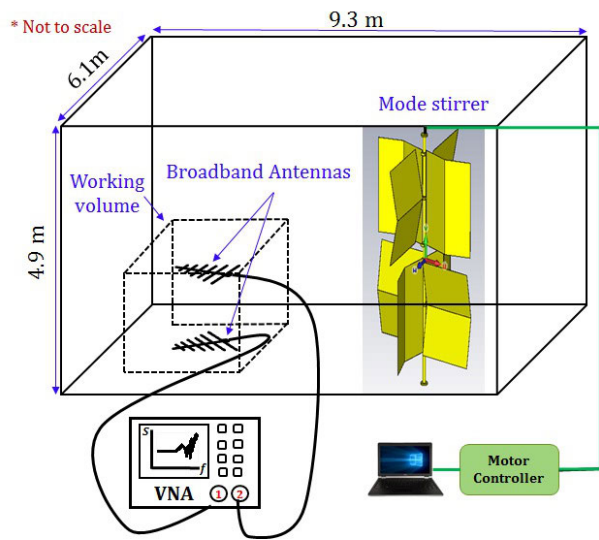

FIGURE 11. Experimental setup for two-port *S*-parameter measurements in RC [51].

FIGURE 12. Principles of determination of critical frequencies: (a) f_{AD} based on interpolated fitted AD GOF statistics, (b) f_{ADRR} based on AD GOF rejection ratio, and (c) f_r based on interpolated fitted $r(1)$.

as 'f_{wso}') involves the assessment of the distribution of EM field and independent samples requirements for the particular stirring condition (*e.g* number of tuner rotations (N)) of the mode-stirred RC. The recorded S-parameters or $|T_I(j\omega)|$ represents the environmental characteristics of the RC and thus can be used for the estimation of the well-stirred condition *i.e.* f_{wso} of the RC in a very short time.

The reported procedure of [17], [22], [50], [51] is based on the null hypothesis (H_o): the distribution of the magnitude of $|S_{11}|/|S_{21}|/|T_I(j\omega)|$ across all stirrer rotations (N) for each frequency, follows the Rayleigh distribution and samples are independent. The pictorial illustration of the above-explained principle is given in Fig. 12.

The assessment of the EM field distribution is done by matching the distribution of $|S_{11}|/|S_{21}|/|T_I(j\omega)|$ with

Rayleigh distribution using high order goodness of fit AD test. The AD test statistics and rejection ratio results are compared with theoretical threshold limits for matching with Rayleigh distribution [42]. Table 3 summarizes the critical values for various distributions based on the number of stirrer rotations (N) and confidence/significance level. This comparison produces the two critical frequencies f_{AD} and f_{ADRR}, respectively as illustrated in Fig. 12.

Subsequently, the f_{wso} is determined by taking the largest of all three critical frequencies *i.e.* f_{AD}, f_{ADRR} and f_r. The largest value is chosen to meet the distribution matching and independent sample requirements for the well-stirred condition of an RC. The f_{wso} can also be computed by taking the largest value of f_{AD} and f_r as reported in [17] as the rejection ratio results are being derived from the AD-GOF test statistics.

Figure 13 shows the waveform of AD-GOF statistic for the measured S_{11} [17], S_{21} [22] and $T_I(\omega)$ [50], [51] data of empty RRA RC with $N = 50$. The results of Fig. 13 are recorded for the frequency range of 80 MHz to 3000 MHz with 29,200 discrete frequency samples. Table 5 depicts the comparison of the determined f_{wso} using S_{11} [17], S_{21} [22] and $T_I(j\omega)$ [50], [51] for the RRA RC. It is pertinent to mention here that the E-field results are compared in Fig. 13 and Table 5 for brevity only. The one-to-one comparison between the computed f_{wso} using E-field and S-parameters data cannot be made as the E-field constitutes of both stirred and unstirred components of RC field. It is difficult to separate the stirred and unstirred components of E-field from the recorded data using the commercially available E-field probes. If the data could be separated with the availability of advanced E-field probes then the proposed method in [17], [22], [50], [51] could be used for the direct comparison of the determined well-stirred condition of RC using E-field and S-parameter data.
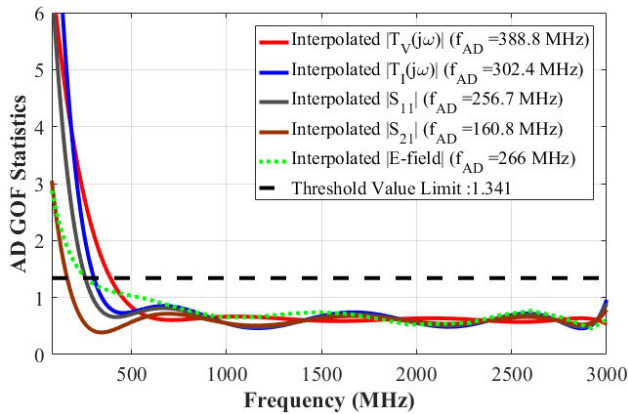
FIGURE 13. Determination of f_{AD} using S_{11} [17], S_{21} [22] and $T_I(\omega)$ [50], [51] data of an empty RC.

The independent samples requirement is checked by computing the first-order auto-correlation ($r(1)$) for each metric and comparing the output results with the threshold limit based on N [43]. The $r(1)$ metric is used for the assessment of the independence of the samples and tuner efficiency *i.e.* received data for each stirrer position is independent of the previous stirrer position. For an ideal RC, data must be highly independent of stirring approach. The $r(1)$ is compared with threshold limit of Table 4 to predict the third critical frequency *i.e.* f_r as shown in Fig. 12.

We note from Table 5 that the determined f_{wso} using S_{11} have relatively good agreement with the predicted f_{wso} using averaged E-field data ($\langle |E| \rangle_{24}$) (see details in [22]). The

TABLE 5. Comparison of estimation of f_{wso} (in MHz) using transfer function $T_I(j\omega)$ [50], [51], E-field, S_{11} [17], and S_{21} [22] results for an empty RC.

	f_{AD}	f_{ADRR}	f_r	f_{wso}
$|T_I(j\omega)|$	302	297	109	302
$\langle |E| \rangle_{24}$	266	302	80	302
$|S_{11}|$	257	319	104	319
$|S_{21}|$	161	116	110	161

compared S_{11} data is obtained by placing only one antenna in RRA RC as suggested in [17]. However, the only transfer function characteristics (S_{21}) did not accurately predict the well-stirred condition of the RC as the obtained value of f_{wso} in this case is 161 MHz. The loading of the RC due to second-placed antenna and stronger low-frequency coupling between the two placed antennas in RC for two-port S-parameter measurements are the reasons of getting relatively lower f_{wso} using S_{21} data. The findings of [50], [51] and as illustrated in Table 5 confirms that when the estimation of the well-stirred condition of the RC is required with the essential placement of the two antennas in RC as needed in [2], [7]–[10], [52], the use of the current gain transfer function of the RC environment is more appropriate. The estimated f_{wso} using $T_I(j\omega)$ and $\langle |E| \rangle_{24}$ is almost same. The current gain transfer function of [50], [51] includes the effect of both environment and antenna transfer characteristics in it. Thus it results in more accurate prediction of the actual overmodded condition of RC as compared to only S_{21} data.

Another interesting thing can be noted from Table 5 that the computed f_{wso} using averaged E-field is 302 MHz while the determined $f_{LUF_{IEC}}$ using field uniformity measurements was around 250 MHz (see Fig. 6). It shows that the $f_{LUF_{IEC}}$ did not accurately predict the over-moded condition of RC as the statistical field uniformity and isotropy of the RC is not exactly achieved at $f_{LUF_{IEC}}$, but rather at little higher than the $f_{LUF_{IEC}}$ due to the associated losses and inherent uncertainties of RC. These losses affect the statistics of the EM field and overmoded condition in RC [40], [53], [54]. Table 6 summarizes the reviewed techniques for the rapid in-direct characterization of an RC.

The reported uncertainly of the proposed procedures of [17], [50], [51] due to the change in antenna type, antenna position, and post-processing of the data is also low (< 5-10%). The researcher had suggested that the estimation of f_{wso} using S_{11} for a single antenna in RC [17] and $T_I(j\omega)$ [50], [51] for the two-antennas in RC could be used as a potential alternative validation procedure of an RC. The operational overmoded condition of the RC could be estimated from f_{wso}. The advantage of these methods [17], [50], [51] is the rapid characterization of the operational requirements of an RC. Additionally, the quick analysis of any change in RC in terms of change in a stirrer position, installation of a new stirrer, working volume size, and loading conditions *etc.* can be performed by rapidly analyzing the variations in the f_{wso} for each case.

The role of the calibration plane is vital for the accuracy of the determined well-stirred condition of RC using [17], [22],

Reference	Year	Summary
S_{21} [22]	2017	o Suitable for RC applications where two antennas are required for onward testings o Inaccurate prediction of the well-stirred condition due to chamber loading
S_{11} [17]	2018	o Suitable for RC applications where only one antenna is required for onward testings
$T_I (j\omega)$ [50], [51]	2020	o Suitable for RC applications where one/two antennas are required for onward testings o Accurate prediction of the well-stirred condition with the minimization of the chamber loading

[50], [51] procedures. The calibration plane must be shifted at the input terminals of the installed antennas in an RC before recording the S-parameter measurements as specified in [17], [22], [50], [51]. The measurement of the small values of S-parameters (particularly of the small values of reflection coefficient) at microwave frequencies with calibration plane at the end of sufficiently long cables enhances the measurement uncertainty. The measurement uncertainty increases with the decrease in the amplitude of the recorded S-parameters which could result in inaccurate estimation of the well-stirred condition of an RC using the proposed procedures of [17], [22], [50], [51].

V. ESTIMATION OF CHAMBER QUALITY FACTOR

Quality factor (Q) represents the RC ability to store the energy relative to its rate of dissipation. Q is an important characterization parameter of RC as it is used for the various applications such as chamber loading analysis; field enhancement in electromagnetic susceptibility (EMS) measurements; decay time constant (τ_{RC}) measurements for the realization of the multipath channel environment; and measurement of absorption cross-section (ACS) of lossy objects. Q and τ_{RC} are interrelated as shown in (8) [55]–[57].

$$Q = 2\pi \frac{W_s}{W_d} = 2\pi \frac{W_s}{P_d T} = \omega \frac{W_s}{P_d} = 2\pi f \tau_{RC} \quad (8)$$

In (8), ω is the angular frequency, W_s is stored energy in RC, W_d is the dissipated energy in one period time (T), and P_d is the dissipated power in the chamber walls. P_d constitutes of power received by the antenna and the power dissipated in RC walls including stirrer.

Wang *et al.* [33] proposed the estimation of the Q using average value of the magnitude of the normalized electric field vector of RC for all stirrer conditions (see 9). In 9 *a*, *b*, and *c* are the RC dimensions which can be multiplied to get volume (V) and ε represents the permittivity of the medium filling the RC cavity.

$$Q = \frac{\varepsilon \omega}{2} \int_0^a \int_0^b \int_0^c |\langle \bar{E} \rangle|^2 \, dxdydz = \frac{1}{2}\varepsilon \omega V |\langle \bar{E} \rangle|^2 \quad (9)$$

The factors like leakage and the presence of dissipative structures like wooden table or flour reduce the quality factor of the cavity. The conductivity of the chamber walls have direct influence on chamber Q. A very high Q may generate spatial field uniformity distribution issues at low frequencies and also enhances the decay time which in turn requires longer relaxation time for the pulse excitation in RC.

It deduces that chamber Q must be optimized to reach on an acceptable requirements of input power along with the meeting of the chamber operational performance requirements.

Chamber quality factor is affected by four major loses: (i) power dissipation in walls; (ii) presence of absorbing object in RC; (iii) aperture leakage; and (iv) power dissipation in the receiving antenna load [55], [56], [58]. The composite quality factor (Q) for the empty chamber is the combination of the quality factor of walls and placed antennas as illustrated in (10) [55], [56], [58].

$$\frac{1}{Q} = \frac{1}{Q_W} + \frac{1}{Q_{Antenna}} \quad (10)$$

A. THEORETICAL CALCULATIONS

There are different reported mathematical expressions for the calculation of the theoretical Q of RC. In 1983, Liu *et al.* [56] reported the (11) for the estimation of the chamber walls Q for a rectangular cavity. In (11), L, W, H are chamber dimensions, $V = LWH$ represents chamber volume, $S = 2(WL + HL + HW)$ is the surface area of the cavity, $\delta = 1/\sqrt{\pi f \sigma_W \mu_o \mu_r}$ represents skin depth with σ_W as conductivity of the wall materials, and $k = \omega/c$. Later on, in 1996, Hill [55] proposed the simplified expression of (11) using the plane wave decomposition for arbitrary shape RC of having non-magnetic walls *i.e.* $\mu_r = 0$. The reported expression of [55] is illustrated in (12)

$$Q_W = \frac{3V}{2\delta S} \frac{1}{1 + \frac{3\pi}{8k}\left(\frac{1}{L} + \frac{1}{W} + \frac{1}{H}\right)} \quad (11)$$

$$Q_W = \frac{3V}{2\delta S} \quad (12)$$

$$Q_{Antenna} = \frac{16\pi^2}{m} \frac{V}{\lambda^3} \quad (13)$$

Besnier *et al.* [58] reported a simple expression (13) for the computation of $Q_{Antenna}$. In (13), m represents the antenna mismatch and it is equal to 1 for matched antenna case. The composite Q can then be calculated using (10) by combing $Q_{Antenna}$ and Q_W.

Figure 14 shows the comparison of the calculated Q_W using and (11) and (12) with $\sigma_W = 3.77e7$ for the Aluminum walls of RRA RC. At high frequency, k becomes larges which simplify the (11) to (12), as can be noted from Fig. 14, where the two curves become identical as the frequency increases. The results of calculated composite Q by including the $Q_{Antenna}$ (13) factor as depicted in Fig. 15. Figure 15 depicts that the low-frequency differences between the two
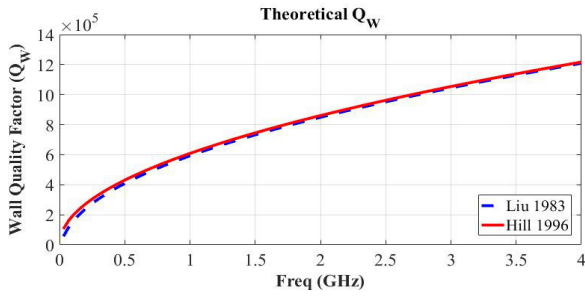
FIGURE 14. Comparison of theoretically computed Q_W using (11) and (12).
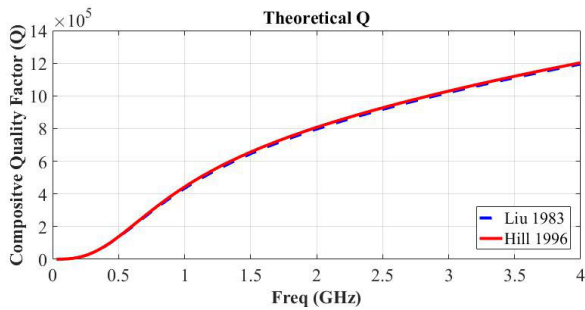

FIGURE 15. Comparison of theoretically computed composite Q using (11), (12) and (13).

curves (see Fig. 14) are reduced by including the antenna quality factor in the wall quality factor.

In [59], the authors had reported the two theoretical expressions as the baseline for an effective RC and suggested that the actual chamber Q must be higher than the computed value using proposed formulas to meet the minimum criterion of an effective chamber. The stringent expression proposed in [59] is illustrated in (14). The calculated Q_{thr} using (14) at 50 MHz for RRA RC is 0.73 while the predicted composite Q using (10) is 1.05e5 which meets the requirements that the actual calculated Q is higher than Q_{thr}.

$$Q_{thr} = \left(\frac{4\pi}{3}\right)^{2/3} \frac{V^{1/3}}{2\lambda} \qquad (14)$$

It is imperative to mention here that the actual measured Q of the chamber will be almost on average 5-10 times higher than the predicated theoretical composite Q using (10) [8], [24], [55], [56], [58], [60]. The main reason for this difference is associated with losses of gaskets which are used in RC assembly and stirrer factors, as their contributions are not included in the simplified expressions of (11) and (12).

B. EXPERIMENTAL CALCULATIONS

Analytical expressions presented in Section V-A are used for the rough estimation of the chamber Q without the incorporation of losses associated with installed stirrers and gaskets in realized RC. Consequentially, the experimental techniques are used for the measurement of the real-time composite Q of the RC for the further usage in field enhancement/decay time calculations. The measurement techniques

of RC Q can be categorized into two main branches: frequency- and time-domain techniques. A brief review of these two approaches is presented here.

1) FREQUENCY DOMAIN Q

In the conventional way of RC decay time (τ_{RC}) calculations, a pulse modulated signal is transmitted in the cavity using a transmitting antenna, and a power meter or oscilloscope is used to record the received signal power at the receiver antenna terminal [61]. Chamber decay time (τ_{RC}) and quality factor can be calculated using the measured S-parameter data. Frequency domain measurements are more suitable due to the higher dynamic range of VNA as well as fast measurements using VNA for the different loading configuration of the chamber.

S-parameters are recorded by placing a single [17] (see Fig. 1 in [17]) or two antennas in an RC [2], [8], [9], [52], [61]–[64] as illustrated in Fig. 11. The data is recorded for the variations (N) in the chosen stirring procedure. Before the measurements, the reference plane must be shifted at the input terminals of antennas through VNA calibration. The recorded S-parameters are saved for each step of stirring procedure (e.g. each stirrer angle). S-parameters must be calculated in the steady-state condition of stirrer, not during the rotation of the stirrers [7], [8], [61]. Also, the VSWR of the measurements antennas must be less than 2 for the operational frequency bands [65].

Q of the chamber can be calculated using (15) [7], [8] for the average received power P_{AveRec} at the receiving antenna terminal for the input power of P_{Input}. The Q is averaged for all rotations (N) of the tuner.

$$Q_{FD} = Q_{Antenna} \left\langle \frac{P_{AveRec}}{P_{Input}} \right\rangle_N \qquad (15)$$

P_{AveRec}/P_{Input} can be replaced with $|S_{21}|^2$ to form (16) with $Q_{Antenna}$ from (13).

$$Q_{FDS21} = \frac{16\pi^2 V}{\lambda^3} \left\langle |S_{21}|^2 \right\rangle_N \qquad (16)$$

Equation (16) can be further modified by adding the corrections for the total efficiencies (η) of the measurement antennas (Tx and Rx) [2], [7], [8] as depicted in (17).

$$Q_{FDS21} = \frac{16\pi^2 V}{\eta_{Tx}\eta_{Rx}\lambda^3} \left\langle |S_{21}|^2 \right\rangle_N \qquad (17)$$

The total antennas efficiencies of the transmit and receiving antennas in an RC are estimated using (18)

$$\eta_{Rx/Rx} = 1 - \left| S_{nn_{Tx/Rx}}^{FS} \right|^2 \qquad (18)$$

In (18), $S_{nn_{Tx/Rx}}^{FS}$ is the free space reflection coefficient of the 'nth' Tx/Rx antenna in free space. It can also be predicted from the measured ensembles averaged reflection coefficient of the antenna in an RC i.e. $S_{nn_{Tx/Rx}}^{FS} \approx \left\langle S_{nn_{Tx/Rx}} \right\rangle_N$. This simplifies the (18) to (19).

$$\eta_{Rx/Rx} \approx 1 - \left| \left\langle S_{nn_{Tx/Rx}} \right\rangle_N \right|^2 \qquad (19)$$
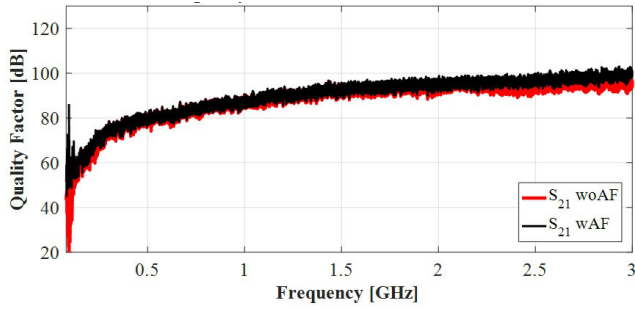
FIGURE 16. Comparison of computed Q_{FD} without (16) and with antenna efficiencies corrections using (17).

FIGURE 17. Comparison of computed Q_{FD} using S_{21} with antenna efficiencies corrections using (17) and S_{11} using (20)/(21).

The quality factor can also be estimated from only single port S-parameter measurements using (20) as reported in [66]. The procedure is applicable even for the case when more than one antennas are present in an RC. In (20), η_o is the wave impedance, ϵ represents the permittivity of the RC propagation medium, and η depicts the efficiency of the antenna which can be estimated using (19). The term $1-|\langle S_{11}\rangle|^2$ in (20) also represents antenna efficiency (see 19). This simplifies (20) to (21).

$$Q_{FD_{S11}} = \left\langle |S_{11} - \langle S_{11}\rangle|^2 \right\rangle \frac{\eta_o \omega \epsilon V}{(\lambda^2/4\pi)\left(1 - |\langle S_{11}\rangle|^2\right)^2 \eta^2} \quad (20)$$

$$Q_{FD_{S11}} = \left\langle |S_{11} - \langle S_{11}\rangle|^2 \right\rangle \frac{\eta_o \omega \epsilon V}{(\lambda^2/4\pi)\,\eta^4} \quad (21)$$

Figure 16 shows the comparison of the computed frequency-domain Q (Q_{FD}) using S_{21} with (17) and without employing the antenna efficiencies correction factors (16) for the frequency range of 80 MHz - 3 GHz. The results of Fig. 16 are with mode-tuned operation of stirrer with $N = 60$. The comparison reflects that the inclusion of the antenna efficiencies affects the determined Q, particularly at low frequencies where the antennas mismatch characteristics reduces the estimated Q values (see red curve). The incorporation of the antenna efficiencies increase the low-frequency Q (see black curve) as depicted in Fig. 16. The comparison of estimated Q_{FD} using S_{21} with incorporated antenna efficient factors (17) and S_{11} using (20)/(21) is shown in Fig. 17. It can be noted from Figs. 16 and 17 that the computed Q using S_{21}-wAF and S_{11} have a better agreement.

2) TIME DOMAIN Q
The estimation of the Q using the time-domain approach is based on an inverse approach. Firstly, decay time (τ_{RC}) of the chamber is computed from the power decay profile (PDP) of the chamber using the chamber impulse response $h(t)$ [67], [68]. Next, τ_{RC} is used to calculate Q_{TD} using (8).

PDP of S_{11} and S_{21} data follows the exponential trend in the time domain [64], [69] i.e. $e^{-t/\tau_{RC}}$. To calculate the PDP (t), firstly the Inverse Fast Fourier transform (IFFT) of the measured frequency domain data (S_{21}/S_{11}) is taken for all stirrer rotations (N) separately. It represents the impulse response '$h(t)$' of (22). Next, the magnitude square of the

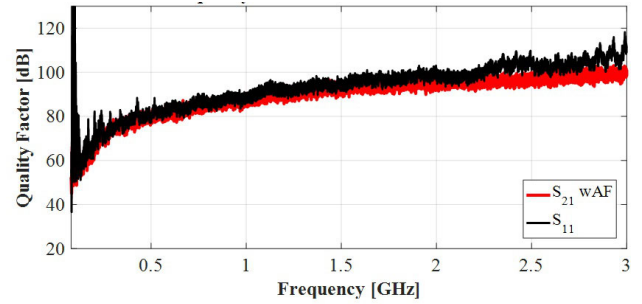IFFT data is taken. After that, its ensemble average for all stirrer rotations is taken to get the PDP (t) as illustrated in (23).

$$PDP(t) = \left\langle |h(t)|^2 \right\rangle_N \quad (22)$$

$$PDP(t) = \left\langle |IFFT(S_{21})|^2 \right\rangle_N = e^{-t/\tau_{RC}} \quad (23)$$

The IFFT is taken for a bandwidth (BW) of data around a center frequency for which Q has to be calculated. This bandwidth is specified based on the pulse duration (τ_p) of the input time domain signal [8], [70]. The pulse duration must be less than wall scattering time ($T_c = 4V/Sc$) of the chamber or decay time of the chamber to minimize the effect of wall losses in computed Q. Usually, the relationship of $BW \geq 2/T_c$ is used for the calculations of the adequate IFFT bandwidth [8], [70], [71]. In Tc, V and S represent the volume and surface area of the chamber while c refers to the speed of light. For RRA RC dimensions, the bandwidth must be higher than 143 MHz as the T_c is 14.01 ns in this case.

Figure 18 shows the PDP of S_{21} data of empty RRA RC. The slope of the PDP (t) represents the trend of the decaying energy in the RC cavity. It is important to mention here that slope is calculated for the stirred or reverberant region using linear square fitting method [8], [64], [72]. The pre-reverberant region represents the antenna excitation and it must be gated out from the linear fitting region to minimize
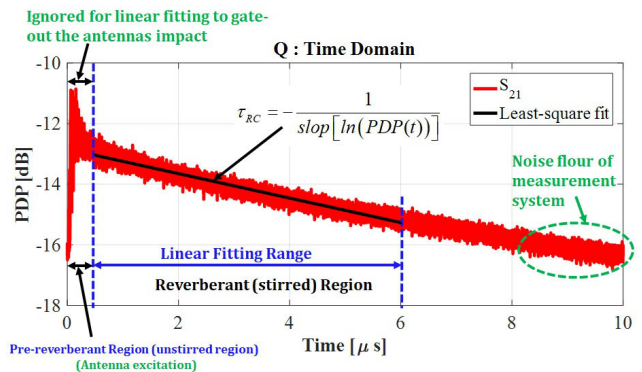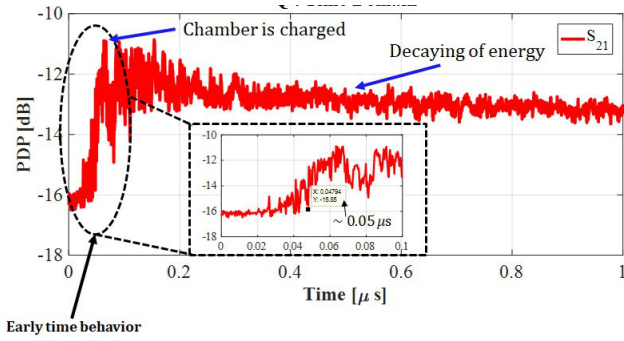

FIGURE 18. PDF of S_{21} data of an empty RC.

FIGURE 19. Early time behavior of an RC in the pre-reverberant region of Fig. 18.

the impact of antenna(s) in computed Q [67], [71]. During this region, the chamber is charging as illustrated in Fig. 19. The chamber is not charged during the early time behavior due to the traveling of the waves on the antenna cables. As depicted in Fig. 19, the under-investigation RC is charged around 0.05 μs. After that decaying of energy is started in RC which follows the exponential pattern. The end of the PDF profile is also ignored for the estimation of the slope as it represents the noise floor of the measurement system. The gating out of antenna impact during the linear fitting provides advantages in time-domain calculation of quality factor as it was removed by incorporating antenna efficiencies in (17) in frequency domain technique [8], [64], [67], [71], [72].

Decay time (τ_{RC}) is calculated by taking the inverse of the slope of the 'dB' scale data of the stirred region as depicted in Fig. 18. τ_{RC} can be computed using two approaches; either by taking natural or common logarithms of the dB data. The procedure of computing τ_{RC} using common logarithm is explained below [8], [64], [67], [71], [72].

$$10log_{10}\left[PDP(t)\right] = 10log_{10}\left(e^{-t/\tau_{RC}}\right)$$
$$10log_{10}\left[PDP(t)\right] = -t/\tau_{RC}\left(10log_{10}\left(e\right)\right)$$
$$10log_{10}\left[PDP(t)\right] = -t/\tau_{RC}\left(4.3429\right)$$
$$\tau_{RC} = \frac{4.3429}{slop\left[10log_{10}\left(PDP(t)\right)\right]} = \frac{4.3429}{D} \quad (24)$$

Following equation can be used for the estimation of τ_{RC} using natural logarithm [52], [61], [68].

$$ln\left[PDP(t)\right] = ln\left(e^{-t/\tau_{RC}}\right)$$
$$ln\left[PDP(t)\right] = -t/\tau_{RC}\left(ln\left(e\right)\right) = -t/\tau_{RC}$$
$$\tau_{RC} = -\frac{1}{slop\left[ln\left(PDP(t)\right)\right]} \quad (25)$$

Normally high possible sampling rate (small sampling interval) is used in frequency domain measurements to assure the accuracy of the recovered time-domain signal with the minimization of the aliasing. Xu *et al.* [61] recorded the data for 10,001 linear sampling point (maximum sample point of their VNA) for the frequency range of 2.0 GHz to 2.1 GHz.

Tian *et al.* [52] used the 10,001 sample points for the frequency range of 3.8 GHz to 5.2 GHz. Table 7 presents the summary of the reviewed studies about the calculation of Q_{FD} and Q_{TD}.

The procedure for the estimation of time constant using S-parameters data is summarized as follows:

- For single/two antenna(s), measured the S_{11}/S_{21} data using VNA for a maximum number of frequency samples for each position of the stirrer. In case of two antennas, second antenna can be terminated with 50 Ω load for S_{11} measurements. Care must be taken to minimize the direct coupling between the antennas to minimize the unstirred field components for S_{21} measurements.
- Use a high-order (*e.g.* 10-order) bandpass elliptic filter to remove the noise/ripples from the signal [52], [61]. Tian *et al.* [52] used the 200 MHz bandwidth filter for this purpose.
- Take the magnitude of an average of the measured S_{11}/S_{21} data for all stirrer rotations or the average can be taken for all the recovered time-domain signals [61].
- Take IFFT of measured data for time-domain S_{11}/S_{21} results keeping in view the T_c constrain.
- Calculate the slope (D) of the time domain results using linear square fitting method (avoid the early-time response for least-square fitting as it may contain unstirred field components due to almost no change in cavity boundary conditions due to on tuner rotation)
- Calculate the τ_{RC} using (24) or (25) and then Q using (8)
- Swap the center frequency of the bandpass filter to calculate the τ_{RC} at different frequencies [52]

The decay time of a loaded chamber is lesser as compared to unloaded chamber [52]. Xu *et al.* [61] also suggested that instead of using large sampling points of the frequency domain data, similar results can be obtained by lower sampling points (large sampling interval (ΔF)) by observing this relationship ($\Delta F \approx 2.73\Delta f$), where Δf is the coherence bandwidth of the cavity. Recently, [72] suggested that the better estimation of the chamber time constant can be done by using non-linear fitting of the PDF(t) to minimize the effect of the employed windowing function while doing a linear square fitting in conventional method [8], [52], [61], [64], [67], [68], [71].

The limitation of the frequency domain calculations of the Q is the inclusion of the antenna factors in the actual measured S-parameters which is hard to separate. This becomes the reason for the different Q values computed using frequency- and time-domain methods. Recently, [8] suggested that the difference between the Q_{FD} and Q_{TD} can be reduced by including the antenna efficiency factors in the frequency domain calculations expression of Q (see Fig. 8 in [8] and Table 2 in [73]). Also, it has been shown by [8] that the accurate prediction of the real-time chamber Q can be done by using the out-of-the band antennas for S-parameter measurements which minimizes the impact of the antenna on the recorded data in the desired frequency range where the reflection characteristics of the antenna are minimum.

TABLE 7. Comparison of reviewed studies about the computation of time-and frequency-domain quality factor (Q).

Reference	Year	Q_{TD}	Q_{FD}	Summary
Nguyen [62]	1999	×	✓	o Analysis of the loading effect of aircraft seats in RC o ACS analysis of complete coach and various seats configurations
Holloway et al. [59]	2006	×	✓	o Derivation of expressions for a threshold chamber Q o Analysis of the effect of loading on chamber Q and computation of ACS of spheres
Richardson [70]	2008	✓	×	o Pulse duration must be less than wall scattering time for Q_{TD} calculations o Analyze the impact of various loadings on the decay time of RC
Genender et al. [67]	2010	✓	×	o Calculation of decay time using S_{21} data for various loading conditions o Characterization of the multipath channel environment in RC using bit error rate (BER)
Rajamani et al. [73]	2012	✓	✓	o Comparison of Q_{TD} and Q_{FD} using S_{21} data o Analyze the impact of impedance mismatch, antenna efficiency and antenna type on Q
Holloway et al. [2]	2012	✓	×	o Computation of Q_{TD} using S_{11}/S_{21} data o Analysis of antenna efficiency measurement using various antenna approaches
Besnier et al. [66]	2015	×	✓	o Estimation of composite Q_{FD} using S_{11}/S_{21} data o Analysis of the impact of antennas on computed Q
Wang et al. [33]	2013	×	✓	o Estimation of Q_{FD} using E-field data using (9) o Analysis of the impact stirring conditions on Q
Xu et al. [61]	2016	✓	×	o Extraction of decay constant without satisfying nyquist criterion using S_{21} data o Sampling interval of recorded data could be larger than the coherence bandwidth of RC
Tian et al. [52]	2016	✓	×	o Computation of Q_{TD} using S_{21} data o ACS analysis of lossy objects in RC without the needs of antenna calibration
Zhang et al. [72]	2017	✓	×	o Usage of non-linear curve fitting and various windowing functions for Q_{TD} using S_{21} data o Comparison of ACS determination of a sphere using linear/non-linear fitting
Nourshamsi et al. [64]	2017	✓	×	o Computation of Q_{TD} using S_{11} data o Analysis of impact of shape of various materials on Q
Nourshamsi et al. [71]	2017	✓	×	o Computation of Q_{TD} using S_{11} data o Detailed analysis of the required bandwidth for the calculation of Q_{TD}
West et al. [8], [36]	2016/2018	✓	✓	o Comparison of computed Q_{TD} and Q_{FD} from S_{21} data o Q_{FD} calculation with the incorporation of antenna efficiency factors o Usage of out-of-band antennas to minimize the impact of antennas in measured Q
Andrieu et al. [68]	2018	✓	×	o Compute the average composite Q of a thermal vacuum chamber (TVC) using S_{11} data o Characterize the performance of TVC using [17] procedure
Xu et al. [69]	2019	✓	×	o Calculation of Q using S_{21} data o Impact of TD error on computed Q due to variaitons in frequency samples rate

* Time-domain (TD), frequency-domain (FD), absorption cross section (ACS)

VI. CONCLUSION

This work has presented a comprehensive review of the various theoretical and experimental techniques for the characterization of the reverberation chamber. The study summarized the analytical and experimental procures for the estimation of the lowest usable frequency (LUF), characterization of the random EM-field using full-wave EM modeling and statistical tests, and computation of the quality factor/time constant of an RC. A comprehensive review of the recently proposed techniques of indirect fast validation of the well-stirred condition of the RC using S-parameter measurements is also presented. The presented work could be beneficial for the EMI/EMC, antenna and qualifications personnel as well as RC students with a quick review of the major old and new techniques for the RC characterizations.

REFERENCES

[1] H. A. Mendes, "A new approach to electromagnetic field-strength measurements in shield enclosures," Wescon, Gurugram, Haryana, Tech. Rep., 1968, pp. 20–23.

[2] C. L. Holloway, H. A. Shah, R. J. Pirkl, W. F. Young, D. A. Hill, and J. Ladbury, "Reverberation chamber techniques for determining the radiation and total efficiency of antennas," IEEE Trans. Antennas Propag., vol. 60, no. 4, pp. 1758–1770, Apr. 2012.

[3] R. Serra, "Reverberation chambers through the magnifying glass: An overview and classification of performance indicators," IEEE Electromagn. Compat. Mag., vol. 6, no. 2, pp. 76–88, Aug. 2017.

[4] V. Mariani Primiani, P. Russo, and G. Cerri, "Design and testing of an antenna system for the source stirring technique in reverberation chambers," J. Electromagn. Waves Appl., vol. 26, no. 7, pp. 837–850, May 2012.

[5] X. Chen, J. Tang, T. Li, S. Zhu, Y. Ren, Z. Zhang, and A. Zhang, "Reverberation chambers for over-the-air tests: An overview of two decades of research," IEEE Access, vol. 6, pp. 49129–49143, 2018.

[6] W. Xue, X. Chen, M. Zhang, L. Zhao, A. Zhang, and Y. Huang, "Statistical analysis of antenna efficiency measurements with non-reference antenna methods in a reverberation chamber," IEEE Access, vol. 8, pp. 113967–113980, 2020.

[7] Electromagnatice Compatibility (EMC)—Part 4–21: Testing and Measurement Techniques-Reverberation Chamber Test Methods, Standard 61000-4-21, 2011.

[8] J. C. West, J. N. Dixon, N. Nourshamsi, D. K. Das, and C. F. Bunting, "Best practices in measuring the quality factor of a reverberation chamber," IEEE Trans. Electromagn. Compat., vol. 60, no. 3, pp. 564–571, Jun. 2018.

[9] C. L. Holloway, D. A. Hill, J. M. Ladbury, P. F. Wilson, G. Koepke, and J. Coder, "On the use of reverberation chambers to simulate a rician radio environment for the testing of wireless devices," *IEEE Trans. Antennas Propag.*, vol. 54, no. 11, pp. 3167–3177, Nov. 2006.

[10] C. Lemoine, E. Amador, and P. Besnier, "On the *K*-factor estimation for rician channel simulated in reverberation chamber," *IEEE Trans. Antennas Propag.*, vol. 59, no. 3, pp. 1003–1012, Mar. 2011.

[11] P. Corona, J. Ladbury, and G. Latmiral, "Reverberation-chamber research-then and now: A review of early work and comparison with current understanding," *IEEE Trans. Electromagn. Compat.*, vol. 44, no. 1, pp. 87–94, Dec. 2002.

[12] D. A. Hill, "Plane wave integral representation for fields in reverberation chambers," *IEEE Trans. Electromagn. Compat.*, vol. 40, no. 3, pp. 209–217, Aug. 1998.

[13] P. Corona, G. Ferrara, and M. Migliaccio, "Reverberating chamber electromagnetic field in presence of an unstirred component," *IEEE Trans. Electromagn. Compat.*, vol. 42, no. 2, pp. 111–115, May 2000.

[14] L. Garcia-Garcia, B. Lindmark, N. Jalden, and C. Orlenius, "Mimo capacity of antenna arrays evaluated using radio channel measurements, reverberation chamber and radiation patterns," *IET Microw., Antennas Propag.*, vol. 1, no. 6, pp. 1160–1169, Dec. 2007.

[15] P. Corona, G. Ferrara, and M. Migliaccio, "Reverberating chambers as sources of stochastic electromagnetic fields," *IEEE Trans. Electromagn. Compat.*, vol. 38, no. 3, pp. 348–356, Aug. 1996.

[16] P. Corona, G. Ferrara, and M. Migliaccio, "A spectral approach for the determination of the reverberating chamber quality factor," *IEEE Trans. Electromagn. Compat.*, vol. 40, no. 2, pp. 145–153, May 1998.

[17] G. Andrieu, N. Ticaud, F. Lescoat, and L. Trougnou, "Fast and accurate assessment of the," well stirred condition" of a reverberation chamber from s_{11} measurements," *IEEE Trans. Electromagn. Compat.*, vol. 61, no. 4, pp. 974–982, 2019.

[18] R. Vogt-Ardatjew, U. Lundgren, S. F. Romero, and F. Leferink, "On-site radiated emissions measurements in semireverberant environments," *IEEE Trans. Electromagn. Compat.*, vol. 59, no. 3, pp. 770–778, Jun. 2017.

[19] H. Sun, C. Gu, Z. Li, Q. Xu, J. Song, B. Xu, X. Dong, K. Wang, and F. Martín, "Enhancing the number of modes in metasurfaced reverberation chambers for field uniformity improvement," *Sensors*, vol. 18, no. 10, p. 3301, Oct. 2018.

[20] L. Musso, F. Canavero, B. Demoulin, and V. Berat, "Radiated immunity testing of a device with an external wire: Repeatability of reverberation chamber results and correlation with anechoic chamber results," in *Proc. IEEE Symp. Electromagn. Compat.*, 2003, pp. 828–833.

[21] H. Streitwolf, R. Heinrich, H.-G. Behnke, L. Dallwitz, and U. Karsten, "Comparison of radiated immunity tests in different EMC test facilities," in *Proc. 18th Int. Zurich Symp. Electromagn. Compat.*, Sep. 2007, pp. 229–232.

[22] G. Andrieu, "Calibration of reverberation chambers from S21 measurements," in *Proc. IEEE Int. Symp. Electromagn. Compat. Signal/Power Integrity (EMCSI)*, Aug. 2017, pp. 675–680.

[23] J. Yousaf, H. Lee, M. Faisal, HanJunee, W. Nah, H. Shahwani, S. A. Shah, and J. G. Yang, "Design, analysis, and validation of rra reverberation chamber," *Int. J. Commun. Syst.*, vol. 4, pp. 1–16, May 2020.

[24] L. R. Arnaut, "Operation of electromagnetic reverberation chambers with wave diffractors at relatively low frequencies," *IEEE Trans. Electromagn. Compat.*, vol. 43, no. 4, pp. 637–653, Nov. 2001.

[25] D. Mandaris, R. Vogt-Ardatjew, E. Suthau, and F. Leferink, "Simultaneous multi-probe measurements for rapid evaluation of reverberation chambers," in *Proc. IEEE Asia–Pacific Symp. Electromagn. Compat. (EMC/APEMC)*, May 2018, pp. 590–594.

[26] C. Bruns and R. Vahldieck, "A closer look at reverberation chambers-3-D simulation and experimental verification," *IEEE Trans. Electromagn. Compat.*, vol. 47, no. 3, pp. 612–626, Aug. 2005.

[27] L. Xiaoqiang, W. Guanghui, Z. Yongqiang, and Z. Chenghuai, "Effects of stirrer on the field uniformity at low frequency in a reverberation chamber and its simulation," in *Proc. Int. Symp. Comput. Sci. Comput. Technol.*, 2008, pp. 517–519.

[28] W. J. Krzysztofik, "Susceptibility of small reverberation chamber investigation," in *Proc. 3rd Eur. Conf. Antennas Propag.*, 2009, pp. 2221–2225.

[29] H.-J. Asander, G. Eriksson, L. Jansson, and H. Akermark, "Field uniformity analysis of a mode stirred reverberation chamber using high resolution computational modeling," in *Proc. IEEE Int. Symp. Electromagn. Compat.*, 2002, pp. 285–290.

[30] V. Mariani Primiani and F. Moglie, "Numerical simulation of reverberation chamber parameters affecting the received power statistics," *IEEE Trans. Electromagn. Compat.*, vol. 54, no. 3, pp. 522–532, Jun. 2012.

[31] F. Moglie and V. M. Primiani, "Numerical analysis of a new location for the working volume inside a reverberation chamber," *IEEE Trans. Electromagn. Compat.*, vol. 54, no. 2, pp. 238–245, Apr. 2012.

[32] S. Wu, Y. Guan, J. Hu, L. Wang, and H. Tang, "Simulation of field uniformity in a reverberation chamber," in *Proc. 3rd Int. Conf. Comput. Sci. Netw. Technol.*, Oct. 2013, pp. 707–710.

[33] S. Wang, Z. C. Wu, G. H. Wei, Y. Z. Cui, and L. S. Fan, "A new method of evaluating reverberation chamber q-factor with experimental validation," *Prog. Electromagn. Res. Lett.*, vol. 36, pp. 103–112, 2013.

[34] A. Ubin, R. Vogt-Ardatjew, F. Leferink, M. Z. Mohd Jenu, and S. Van De Beek, "Statistical analysis of three different stirrer designs in a reverberation chamber," in *Proc. Asia–Pacific Symp. Electromagn. Compat. (APEMC)*, May 2015, pp. 604–607.

[35] A. N. Bakti, J.-Y. Kwon, J.-H. Choi, and N.-W. Kang, "Design and measurement of the KRISS reverberation chamber 1," in *Proc. Asia–Pacific Radio Sci. Conf. (URSI AP-RASC)*, Aug. 2016, pp. 1765–1768.

[36] J. C. West, V. Rajamani, and C. F. Bunting, "Frequency- and time-domain measurement of reverberation chamber Q: An in-silico analysis," in *Proc. IEEE Int. Symp. Electromagn. Compat. (EMC)*, Jul. 2016, pp. 7–12.

[37] J. Yousaf, H. Lee, H. Junhee, J. Kim, M. Faisal, J. G. Yang, and W. Nah, "Analysis of effect of stirrer type on field uniformity in rra reverberation chamber," in *2018 Int. Symp. Antennas Propag. (ISAP)*, 2018, pp. 1–2.

[38] F. Moglie, "Convergence of the reverberation chambers to the equilibrium analyzed with the finite-difference time-domain algorithm," *IEEE Trans. Electromagn. Compat.*, vol. 46, no. 3, pp. 469–476, Aug. 2004.

[39] A. Adardour, G. Andrieu, and A. Reineix, "On the low-frequency optimization of reverberation chambers," *IEEE Trans. Electromagn. Compat.*, vol. 56, no. 2, pp. 266–275, Apr. 2014.

[40] C. Lemoine, P. Besnier, and M. Drissi, "Investigation of reverberation chamber measurements through high-power Goodness-of-Fit tests," *IEEE Trans. Electromagn. Compat.*, vol. 49, no. 4, pp. 745–755, Nov. 2007.

[41] G. Andrieu, "Calibration of reverberation chambers from S11 measurements," in *Proc. Int. Symp. Electromagn. Compat.*, Sep. 2017, pp. 1–6.

[42] M. A. Stephens, "EDF statistics for goodness of fit and some comparisons," *J. Amer. Stat. Assoc.*, vol. 69, no. 347, pp. 730–737, Sep. 1974.

[43] O. Lunden and M. Backstrom, "Stirrer efficiency in FOA reverberation chambers. Evaluation of correlation coefficients and chi-squared tests," in *Proc. IEEE Int. Symp. Electromagn. Compat.*, 2000, pp. 11–16.

[44] A. Gifuni, "Deterministic approach to estimate the upper bound of the electric field in a reverberation chamber," *IEEE Trans. Electromagn. Compat.*, vol. 53, no. 3, pp. 570–578, Aug. 2011.

[45] T. H. Lehman and G. J. Freyer, "Characterization of the maximum test level in a reverberation chamber," in *Proc. IEEE Int. Symp. Electromagn. Compat.*, 1997, pp. 44–47.

[46] N. Wellander, O. Lunden, and M. Backstrom, "The maximum value distribution in a reverberation chamber," in *Proc. IEEE EMC Int. Symp. Rec.*, 2001, pp. 751–756.

[47] G. Orjubin, "Maximum field inside a reverberation chamber modeled by the generalized extreme value distribution," *IEEE Trans. Electromagn. Compat.*, vol. 49, no. 1, pp. 104–113, Feb. 2007.

[48] J. M. Ladbury, G. H. Koepke, and D. G. Camell, "Evaluation of the nasa langley research center mode-stirred chamber facility," Nat. Inst. Standards Technol. (NIST), Gaithersburg, MD, USA, Tech. Rep. NIST TN-1508, 1999.

[49] P. F. Wilson, D. A. Hill, and C. L. Holloway, "On determining the maximum emissions from electrically large sources," *IEEE Trans. Electromagn. Compat.*, vol. 44, no. 1, pp. 79–86, 2002.

[50] J. Yousaf, M. Ghazal, M. N. Hasan, H. Lee, W. Nah, and J. G. Yang, "Rapid alternative calibration procedure of reverberation chamber using coupling transfer gain function," in *Proc. IEEE Int. Symp. Antennas Propag. North Amer. Radio Sci. Meeting*, 2020, pp. 1–2.

[51] J. Yousaf, M. Ghazal, H. Lee, M. Faisal, J. G. Yang, and W. Nah, "Efficient assessment of well-stirred operation of reverberation chamber using coupling transfer gain functions," *J. Electromagn. Waves Appl.*, vol. 1, no. 5, pp. 1–21, 2020.

[52] Z. Tian, Y. Huang, Q. Xu, T.-H. Loh, and C. Li, "Measurement of absorption cross section of a lossy object in reverberation chamber without the need for calibration," in *Proc. Loughborough Antennas Propag. Conf. (LAPC)*, Nov. 2016, pp. 1–5.

[53] A. K. Fall, P. Besnier, C. Lemoine, M. Zhadobov, and R. Sauleau, "Determining the lowest usable frequency of a frequency-stirred reverberation chamber using modal density," in *Proc. Int. Symp. Electromagn. Compat.*, Sep. 2014, pp. 263–268.

[54] A. Cozza, "The role of losses in the definition of the overmoded condition for reverberation chambers and their statistics," *IEEE Trans. Electromagn. Compat.*, vol. 53, no. 2, pp. 296–307, May 2011.

[55] D. A. Hill, "A reflection coefficient derivation for the q of a reverberation chamber," *IEEE Trans. Electromagn. Compat.*, vol. 38, no. 4, pp. 591–592, Nov. 1996.

[56] B.-H. Liu, D. C. Chang, and M. T. Ma, "Eigenmodes and the composite quality factor of a reverberatingchamber," *Nat. Bureau Standards, Washington, DC, USA, NBS Tech. Note 1066, 1983.

[57] D. A. Hill, M. T. Ma, A. R. Ondrejka, B. F. Riddle, M. L. Crawford, and R. T. Johnk, "Aperture excitation of electrically large, lossy cavities," *IEEE Trans. Electromagn. Compat.*, vol. 36, no. 3, pp. 169–178, 1994.

[58] P. Besnier and B. Démoulin, *Electromagnetic Reverberation Chambers*. Hoboken, NJ, USA: Wiley, 2013.

[59] C. L. Holloway, D. A. Hill, J. M. Ladbury, and G. Koepke, "Requirements for an effective reverberation chamber: Unloaded or loaded," *IEEE Trans. Electromagn. Compat.*, vol. 48, no. 1, pp. 187–194, Feb. 2006.

[60] L. R. Arnaut, "Statistics of the quality factor of a rectangular reverberation chamber," *IEEE Trans. Electromagn. Compat.*, vol. 45, no. 1, pp. 61–76, Feb. 2003.

[61] Q. Xu, Y. Huang, L. Xing, and Z. Tian, "Extract the decay constant of a reverberation chamber without satisfying nyquist criterion," *IEEE Microw. Wireless Compon. Lett.*, vol. 26, no. 3, pp. 153–155, Mar. 2016.

[62] T. Nguyen, "RF loading effects of aircraft seats in an electromagnetic reverberating environment," in *Proc. 18th Digit. Avionics Syst. Conf.*, 1999, p. 10.

[63] X. Zhou, Z. Zhong, X. Bian, R. He, R. Sun, K. Guan, K. Liu, and X. Guo, "Measurement and analysis of channel characteristics in reflective environments at 3.6 GHz and 14.6 GHz," *Appl. Sci.*, vol. 7, no. 2, p. 165, Feb. 2017.

[64] N. Nourshamsi and C. F. Bunting, "Impact of the shape of lossy materials inside a reverberation chamber," in *Proc. IEEE Int. Symp. Electromagn. Compat. Signal/Power Integrity (EMCSI)*, Aug. 2017, pp. 665–669.

[65] A. Gifuni, "Effects of the correction for impedance mismatch on the measurement uncertainty in a reverberation chamber," *IEEE Trans. Electromagn. Compat.*, vol. 57, no. 6, pp. 1724–1727, Dec. 2015.

[66] P. Besnier, C. Lemoine, and J. Sol, "Various estimations of composite Q-factor with antennas in a reverberation chamber," in *Proc. IEEE Int. Symp. Electromagn. Compat. (EMC)*, Aug. 2015, pp. 1223–1227.

[67] E. Genender, C. L. Holloway, K. A. Remley, J. M. Ladbury, G. Koepke, and H. Garbe, "Simulating the multipath channel with a reverberation chamber: Application to bit error rate measurements," *IEEE Trans. Electromagn. Compat.*, vol. 52, no. 4, pp. 766–777, Nov. 2010.

[68] G. Andrieu, N. Ticaud, F. Lescoat, and L. Trougnou, "Radiated susceptibility tests in thermal vacuum chambers working as reverberation chambers," in *Proc. Int. Symp. Electromagn. Compat. (EMC EUROPE)*, Aug. 2018, pp. 1–9.

[69] J. Xu, Y. Zhao, and Q. Xu, "On the time domain error caused by the frequency domain sampling rate in a reverberation chamber," *IEEE Access*, vol. 7, pp. 78223–78227, 2019.

[70] R. E. Richardson, "Reverberant microwave propagation," Naval Surface Warfare Center, Dahlgren, VA, USA, Tech. Rep. 2000-2008, 2008.

[71] N. Nourshamsi, J. C. West, and C. F. Bunting, "Required bandwidth for time-domain measurement of the quality factor of reverberation chambers," in *Proc. IEEE Int. Symp. Electromagn. Compat. Signal/Power Integrity (EMCSI)*, Aug. 2017, pp. 481–485.

[72] X. Zhang, M. P. Robinson, I. D. Flintoft, and J. F. Dawson, "Efficient determination of reverberation chamber time constant," *IEEE Trans. Electromagn. Compat.*, vol. 60, no. 5, pp. 1296–1303, Oct. 2018.

[73] V. Rajamani, C. F. Bunting, and J. C. West, "Differences in quality factor estimation in frequency and time domain," in *Proc. Asia–Pacific Symp. Electromagn. Compat.*, May 2012, pp. 505–508.

JAWAD YOUSAF received the M.S. and Ph.D. degrees in electronics and electrical engineering from Sungkyunkwan University, Suwon, South Korea, in 2016 and 2019 respectively. He is currently working as an Assistant Professor with the Electrical and Computer Engineering Department, Abu Dhabi University, United Arab Emirates. Lastly, he worked as Brain of Korea (BK)-Postdoctoral Fellow in the EMC Laboratory, Sungkyunkwan University, Suwon, South Korea, from March 2019 to July 2019. Previously, he worked as the Senior RF Researcher in the Pakistan Space and Upper Atmosphere Research Commission (SUPARCO: National Space Agency of Pakistan) from 2009 to 2013. His research interests include applications of artificial intelligence in electromagnetic and bio-applications, ESD analysis, reverberation chamber, CP antenna designing and modeling, chipless RFID tags, and EMI/EMC analysis and measurements of the systems for space and commercial environment. His research work has resulted in over 65 publications in leading peer reviewed international technical journals, and refereed international and national conferences.

Dr. Yousaf was a recipient of prestigious Brain of Korea (BK)-21 Post doctorate fellowship 2019, 2nd Best PhD. Graduate Award of collage 2019, Best Paper Award in 49th KIEE Summer Conference 2018, winner of the Grand Prize for Best Paper in 3rd Electromagnetic Measurement Competition of KIESS 2018, Prestigious Annual EMC Scholarship Award of KIEES and EMCIS Company Ltd. 2017, Best EMC Symposium Paper Award, and EDCOM Best Student Paper Award Finalist in 2017 IEEE International Symposium on EMC and SI/PI 2017 (USA).

WANSOO NAH (Member, IEEE) received the B.S., M.S., and Ph.D. degrees in electrical engineering from Seoul National University, South Korea, in 1984, 1986, and 1991, respectively. Since 1995, he has been with Sungkyunkwan University, South Korea, where he is currently a Professor with the College of Information and Communication Engineering. He was a Guest Researcher with the Superconducting Super Collider Laboratory (SSCL), USA, from 1991 to 1993, and was also with the Korea Electrical Research Institute (KERI), Changwon, South Korea, as a Senior Researcher, from 1991 to 1995. His primary interests are electromagnetic interference/compatibility (EMI/EMC) analysis, and signal /power integrity (SI/PI)-aware electric/electronic circuit analysis and design.

MOUSA I. HUSSEIN (Senior Member, IEEE) received the B.Sc. degree in electrical engineering from West Virginia Tech, USA, in 1985, and the M.Sc. and Ph.D. degrees in electrical engineering from the University of Manitoba, Winnipeg, MB, Canada, in 1992 and 1995, respectively. From 1995 to 1997, he was with research and development group at Integrated Engineering Software Inc., Winnipeg, Canada, working on developing EM specialized software based on the Boundary Element method. In 1997, he joined the faculty of engineering at Amman University, Amman, Jordan, as an Assistant Prof. He is currently an Associate Professor with the Electrical Engineering Department, United Arab Emirates University. His current research interests include computational electromagnetics, electromagnetic scattering, antenna analysis and design, metamaterial and applications, and material characterization. He has over 70 publications in international journals and conferences. He supervised several Ph.D. and M.Sc. students.

JUN GYU YANG received the B.S., M.S., and Ph.D. degrees in information and communication engineering from Kunsan National University, South Korea, in 1995, 1997, and 2008, respectively. Since 1997, he has been with the Radio Research Agency of Ministry of Science and ICT, South Korea, where he is currently a Deputy Director of technical regulation division. His primary interests are electromagnetic compatibility (EMC) and telecommunication facility regulations.

AMIR ALTAF (Member, IEEE) received the B.Sc. degree in electrical engineering from the University of Engineering and Technology, Peshawar, Pakistan, in 2011, and the Ph.D. degree from the Division of Electronics and Electrical Engineering, Dongguk University, Seoul, South Korea, in 2018. He is currently working as a Postdoctoral Researcher with the Department of Electrical and Computer Engineering, Sungkyunkwan University, Suwon, South Korea. His research interests include circularly polarized antennas, reconfigurable dielectric resonator antennas, MIMO antennas, and development of millimeter-wave on-chip antennas and passive circuits. He is a member of IEEE Antennas and Propagation Society.

MANZOOR ELAHI received the B.Sc. degree in electrical engineering from the University of Engineering and Technology, Peshawar, Pakistan, in 2011, and the M.S. degree in electrical engineering from COMSATS University, Islamabad, Pakistan, in 2015. He is currently working as a Lecturer with the Electrical and Computer Engineering Department, CUI Pakistan, Sahiwal campus. His research interests include MIMO antennas, circularly polarized antennas, reconfigurable dielectric resonator antennas, and reflectarray antennas.

● ● ●